

Temperature- and flow-enhanced detection specificity of mutated DNA against the wild type with reporter microspheres

Cite this: *Analyst*, 2013, **138**, 6117

Ceyhun E. Kirimli,^a Wei-Heng Shih^b and Wan Y. Shih^{*a}

Detection of mutated (MT) deoxyribonucleic acid (DNA) amongst the wild type (WT) requires the probe DNA (pDNA) that is complementary to the MT to discriminate the WT by one or two nucleotide mismatches. Traditionally this is achieved by raising the temperature to above the melting temperature (T_m) of the WT (T_{WT}) but below that of the MT (T_{MT}). However, a raised temperature is also accompanied by a weakened binding of the MT to the pDNA which can reduce the detection sensitivity. In this study, we investigated flow as a way to enhance MT detection specificity at a lower temperature. Gold-coated glass (GCG) slides immobilized with pDNA complementary to the target MT were placed at the center of the flow cell. The detection was done by flowing MT or WT at various concentrations followed by flowing 10^5 ml^{-1} fluorescent reporter microspheres (FRMs) that were $6 \mu\text{m}$ in size and coated with reporter DNA complementary to the MT or WT but different from the pDNA at various flow rates and temperatures. The detection of MT or WT was characterized by counting the FRMs captured on the GCG. Hepatitis B virus 1762/1764 double mutation (HBV DM) was the model MT and the T_{MT} and T_{WT} were 47°C and 22°C , respectively. It was shown that at room temperature, flow initially increased the binding of both the MT and WT at lower flow rates but decreased the binding at flow rates $\geq 4 \text{ ml min}^{-1}$ due to the increase in the flow-induced impingement force on the FRMs to overcome the binding of the MT and the WT to the GCG at higher flow rates. At $\geq 30^\circ\text{C}$ the decrease in binding of the WT with an increasing flow rate was more than that of the MT because 30°C was above the T_{WT} but still well below the T_{MT} . As a result, the detection of MT at 30°C with a flow rate of 4 ml min^{-1} was more specific than at 35°C without flow. These results indicate that flow can diminish WT binding at a lower temperature than without flow and allow MT detection to occur at a lower temperature with high specificity.

Received 22nd February 2013

Accepted 23rd July 2013

DOI: 10.1039/c3an00384a

www.rsc.org/analyst

Introduction

Cancer is a genetic disease and gene mutation is an important form of genetic defect that plays an important role in cancer pathways. Detecting gene mutation is essential for cancer diagnosis, cancer therapy decision, as well as therapy efficacy monitoring. Many genetic cancer markers are known to circulate in body fluids such as serum and urine. Detecting circulating genetic markers in serum or urine is minimally invasive or non-invasive, which can be an integral part of the therapy monitoring when the primary tumor is removed or hard to get to. One challenge of detecting cancer genetic markers in serum or urine is that the wild type shed by the normal cells may be far more abundant than the defected gene shed by the cancer. For example, the wild type (WT) Kras gene is known to outnumber the mutant (MT) Kras gene by a factor of 240.¹ Gene mutation is

among the most challenging to detect as one must be able to detect and differentiate the MT from the WT given that the WT outnumbers the MT and the genetic difference between the MT and WT is often one nucleotide. Currently WT can be discriminated using methods such as denaturing gradient gel electrophoresis,² temperature gradient gel electrophoresis,³ single strand conformation polymorphisms,⁴⁻⁶ heteroduplex analysis,⁷ chemical cleavage methods,^{8,9} protein truncation tests,^{10,11} DNA chips^{12,13} and high resolution melting temperature analysis.¹⁴ All of the above methods are based on the fact that the hybridization kinetics between the WT and the probe DNA (pDNA) is different from that between the MT and the pDNA. For a pDNA that is perfectly complementary to MT, the melting temperature of the MT, the de-hybridization temperature between the pDNA and the MT, T_{MT} , is higher than the melting temperature of the WT, the de-hybridization temperature between the pDNA and the MT, T_{WT} . This melting temperature difference is important in differentiating the MT from the WT. Typically the MT is detected at a temperature between T_{MT} and T_{WT} .¹⁴⁻¹⁶ While raising the temperature within the T_{MT} - T_{WT} window may minimize the binding of the WT to improve

^aDrexel University, School of Biomedical Engineering, Science, and Health Systems, Philadelphia, Pennsylvania, USA. E-mail: shihwy@drexel.edu

^bDrexel University, Department of Materials Science and Engineering, Philadelphia, Pennsylvania, USA

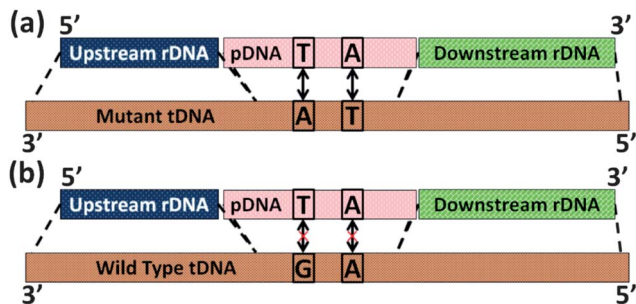


Fig. 1 A schematic of the nucleotide sequences of (a) MT and (b) WT and their hybridization on pDNA, upstream rDNA and downstream rDNA.

specificity; it can also reduce the binding of the MT, thus reducing the sensitivity. Some single-nucleotide mutations may have a $T_{MT}-T_{WT}$ window as small as less than 1°C ,¹⁷ making it difficult to differentiate MT from WT by temperature means alone. Recent development of locked nucleic acid (LNA) pDNA that can help widen the window between T_{MT} and T_{WT} is one way to help better differentiate MT from WT.¹⁸

Fluorescent polystyrene microspheres have been used as a means of detecting DNA hybridization.¹⁹ Furthermore in a systematic study involving shear flow, microspheres were coated with single stranded DNA to hybridize with pDNA on a surface under the influence of various levels of shear stress. It was shown that shear stress played an important role similar to that of temperature in that DNA became increasingly dehybridized with an increasing shear stress and that there existed a critical shear stress above which microspheres became detached from the surface and that DNAs with a single mismatch exhibited a somewhat lower number of attached microspheres per unit area.²⁰ In addition, flow has also been shown to minimize cross-binding of closely related species of *Bacillus anthracis* (BA) such as *B. thuringiensis* (BT), *B. cereus* (BC), and *B. subtilis* (BS) to anti-BA antibody immobilized on a sensor situated at the centre of a laminar flow.²¹ Fluid flow in a narrow channel has also been shown to help enhance detection sensitivity by reducing nonspecific binding.²²⁻²⁴ Therefore, it seems possible that fluid flow may be an auxiliary tool to further improve the specificity of mutation detection.

The purpose of this study was to investigate how flow can affect the specificity of mutation detection in addition to temperature with the help of fluorescent reporter microspheres (FRMs). The model mutant (MT) gene was the 1762T/1764A

HBV double mutation which is present in 50–85% of hepatocellular carcinomas (HCC).²⁵⁻²⁹ The HBV DM MT gene has two mutated sites that are close to each other as shown in the schematic in Fig. 1a and in Table 1. A gold-coated glass (GCG) with pDNA complementary to the MT covalently immobilized on its surface was vertically immersed in the center of a laminar flow of the MT or WT solution for the MT or WT to hybridize to the pDNA on the GCG. Separately, FRMs are covalently coated with reporter DNA (rDNA) that is complementary to MT and WT but different from pDNA (see the schematic in Fig. 1 and Table 1). After MT or WT binding, the GCG was immersed in a flow of FRMs for the FRMs to hybridize to the captured MT or WT on the GCG. By varying the flow rate at various temperatures between T_{MT} and T_{WT} we will be able to determine whether flow helps to improve the specificity of mutation detection.

Experimental

Target DNAs, probe DNA, and reporter DNAs

The MT used in this study was a 200-nucleotide (nt) long single-stranded DNA (Integrated DNA Technologies) containing the nucleotide sequence of the Hepatitis B virus genome (GeneBank Accession #X04615) centered around the 1762T/1764A double mutations.³⁰ Part of the sequence of the MT around the double mutations is shown in Table 1 where the two mutation sites were denoted by underlines. A partial sequence of the 200-nt long WT is also shown in Table 1. 16-nt long synthetic single-stranded pDNA and 30-nt reporter DNA (rDNA) were purchased from Sigma. The pDNA was complementary to MT targeting the 16-nt sequence focused around the double mutation sites of the MT. The sequence of the pDNA is also shown in Table 1. The pDNA was amine-activated and had a 12-polyethyleneglycol (PEG) spacer at the 5' end. The melting temperature of the MT with pDNA was 47°C and that of the WT with pDNA was 23°C as estimated using salt adjustment for phosphate buffered saline ($1\times$ PBS).^{31,32} These two melting temperatures are also listed in Table 1.

There were two different 30-nt long rDNAs. The rDNAs were complementary to the sequence of the MT and WT upstream and downstream of the 16-nt sequence that was complementary to the pDNA. The reason for using two different reporter DNAs was that the present study was aimed at a model study to detect trans-renal DNA in patients' urine samples. Trans-renal DNAs are DNA fragments of less than 200 bps from distant organs. The sequence targeted by the pDNA might not be

Table 1 The sequences of the pDNA, MT, WT, upstream rDNA, downstream rDNA and their corresponding melting temperatures, T_m

Type of DNA	Sequence (5' to 3')	T_m ($^\circ\text{C}$)
MT ^a	5'.....GGTTAA <u>TG</u> ATCTTTGT.....3'	47
WT	5'.....GGTTAAAGGTCTTTGT.....3'	23
pDNA	Amine-5'-ACAAAGATCATTAACC-3'	—
Upstream rDNA	Amine-5'-ACAGACCAATTTATGCCTACAGCCTCCTAG-3'	76.3
Downstream rDNA	5'-AATCTCCTCCCCAACTCCTCCAGTCTTT-3'-amine	77.4

^a Mutation sites are indicated by underlines.

always at the center of the DNA fragments. Including two reporter sequences one upstream and one downstream would ensure that there always be one reporter DNA that could attach to the captured DNA fragments. The upstream rDNA was amine activated with a 12-PEG spacer at the 5' end and the downstream rDNA was also amine activated but with a 7-PEG spacer at the 3' end. The sequence of the upstream rDNA and that of the downstream rDNA are also shown in Table 1. The melting temperature of the upstream rDNA to the MT/WT was 76.3 °C and that of the downstream rDNA to the MT/WT was 77.4 °C. Since the sequences of the WT and MT were identical except for the two mutation sites, the melting temperature of the upstream or downstream rDNA to the WT was the same as that of the upstream or downstream rDNA to the MT. The melting temperatures of the two rDNAs with the MT and those of the rDNA with the WT are also listed in Table 1. Fig. 1a and b show schematics illustrating the relationship between MT, pDNA, and upstream and downstream rDNAs and that between WT, pDNA, and upstream and downstream rDNAs, respectively. The upstream and downstream rDNAs were designed to have much stronger binding to the target MT or WT than the pDNA to the target MT or WT. Therefore, when unbinding due to the flow-induced impingement force occurred it would occur at the binding sites between the pDNA and the MT or WT but not at that between the rDNA and the MT or WT. Because the binding of the pDNA to the WT was much weaker than that of pDNA to the MT, theoretically, the flow-induced impingement force could more easily overcome the weaker binding between the pDNA and the WT than that between the pDNA and the MT to allow us to selectively detect MT but not WT.

Substrate preparation and pDNA immobilization

Glass microscope coverslips (22 mm × 22 mm) were deposited with 100 nm thick gold using thermal evaporation. The coverslips were then cut into small rectangular pieces of approximately 3 mm × 3 mm. In the following we will refer to these 3 mm × 3 mm gold-coated glass coverslips as GCGs. The surface of these GCGs was cleaned by immersing them into 100 times diluted piranha solution (1 : 1 sulfuric acid : hydrogen peroxide by volume) for 2 minutes and then washed with deionized water and anhydrous ethanol. The GCGs were then immersed in 50 ml of 0.01 mM 3-mercaptopropyl trimethoxysilane (MPS) (Sigma) solution in ethanol to coat the MPS on the gold surface of the GCGs. The pDNA was immobilized on the MPS surface using sulfosuccinimidyl-4-(*N*-maleimidomethyl)-cyclohexane-1-carboxylate (sulfo-SMCC) (Pierce) as the bi-function. The maleimide end of the SMCC reacted with the thiol of the MPS on the GCG surface and the NHS ester end of the SMCC reacted with the amine at the 5' end of the pDNA, thereby, covalently immobilized the pDNA on the GCG surface (Fig. 2a). The 12-PEG spacer at the 5' end of the pDNA would allow the pDNA to be at a distance from the GCG surface for easy hybridization to the tDNA. After MPS coating, the MPS-coated GCGs were immersed in a 1 μM pDNA solution with 5 mM sulfo-SMCC for 1 hour to immobilize the pDNA. The GCG was then

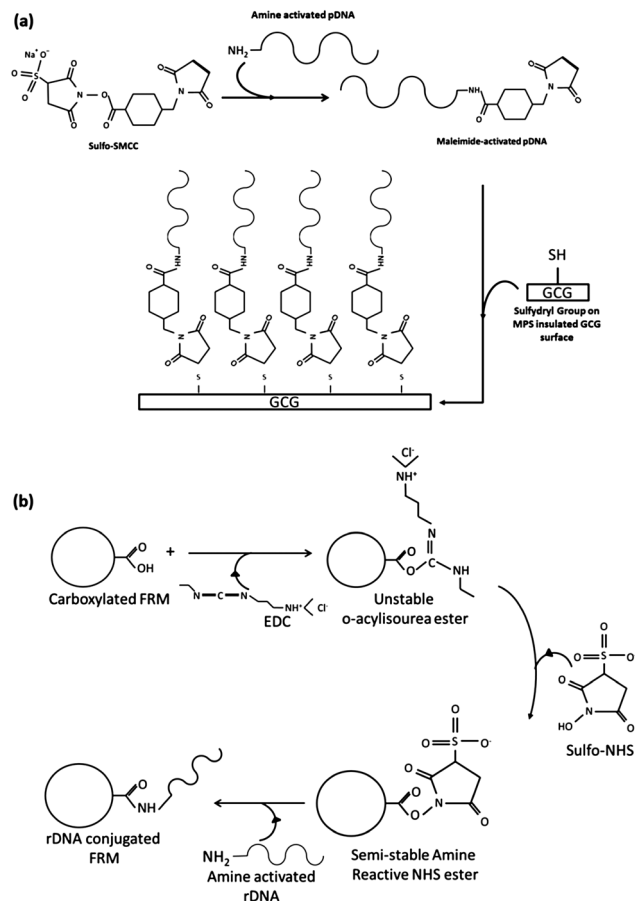


Fig. 2 A schematic of (a) pDNA immobilization on a GCG surface using sulfo-SMCC, and (b) schematic of rDNA conjugation on carboxylated FRMs with sulfo-NHS and EDC.

rinsed with DI water and phosphate buffer saline (PBS) solution and made ready for MT or WT binding.

The gold coating was homogenous as it was done by thermal evaporation at 3.1×10^{-5} torr (Thermionics Vacuum Evaporator, Model VE-90). The gold coating was smooth with a uniform thickness of about 100 nm.³³

A micrograph of a GCG bound with FRMs at 10^5 ml⁻¹ following tDNA detection at 100 pM at room temperature without flow is shown in Fig. 3. As can be seen, the distribution of the FRMs was quite uniform supporting that the distribution of the pDNA on the MPS surface was uniform. The uniformity of the pDNA distribution on the MPS surface was also supported by the visualization of the Cy3-labeled tDNA captured by the pDNA on the MPS of a piezoelectric plate sensor prepared with the same methodology albeit *via* a somewhat different biotin-streptavidin-biotin scheme.³⁴

rDNA conjugation to FRMs

Blue fluorescent polystyrene microspheres (FRMs) (bright blue, excitation: 360 nm, emission: 407 nm) (Polysciences) 6 μm in diameter were conjugated with two rDNAs. First, 0.1 ml of 2.1×10^8 particles per ml of stock suspension of FRMs was diluted



Fig. 3 Fluorescent micrograph of bright blue FRMs on a GCG surface following hybridization of 100 pM of tDNA. Area shown is approximately 1 mm by 1 mm.

10 times in PBS. Afterwards, the suspension went through the following washing steps three times: vortexing for 15 seconds, centrifuging at 3700 rpm (Centra, CL2, IEC, MA), discarding the supernatant, re-suspending the sediment in 10 ml of PBS. For conjugation, FRM suspensions at 2.1×10^6 particles per ml were incubated with 3.3 μM , 330 nM, 33 nM and 3.3 nM of mixed upstream and downstream rDNA solutions at a 1 : 1 ratio with 5 mg ml⁻¹ 1-ethyl-3-(3-dimethylaminopropyl) carbodiimide (EDC) (Sigma, MA) and 5 mg ml⁻¹ sulfonated *N*-hydroxy-succinimide (sulfo-NHS) (Pierce, IL) at pH = 6 at room temperature for 1 h (Fig. 2b). The suspensions were then washed by centrifugation 3 times as described above. After the final washing, 10 ml of four different stock conjugated FRM suspensions at 2.1×10^6 particles per ml were obtained from four different rDNA concentrations. In each experiment, 1 ml of a stock conjugated FRM suspension was further diluted 10 times to a volume of 10 ml and a concentration of 2.1×10^5 particles per ml. In the following, all results were obtained at 2.1×10^5 particles per ml. Overall, due to the high negative charges on the FRMs and the high negative charges of the rDNAs, the FRMs whether conjugated or unconjugated were stable against aggregation as evident in Fig. 3 where the FRMs captured on the surface were well separated supporting that these FRMs did not aggregate in the suspensions. Fig. 4a shows a schematic of a FRM covalently coated with both the upstream and downstream rDNAs.

tDNA hybridization and subsequent capturing of FRMs

Hybridization of the MT or WT to the probe DNA on a GCG and the subsequent hybridization of the FRMs by the bound MT or WT on the GCG were carried out in an open flow cell where the GCG was placed at the center of the detection chamber with the major faces of the GCG parallel to the direction of the flow as schematically shown in Fig. 4b at various temperatures controlled in an incubator (Digital Control Steel Door Incubator 10-180E, Quincy Lab). The custom-made flow cell was 18.5 mm

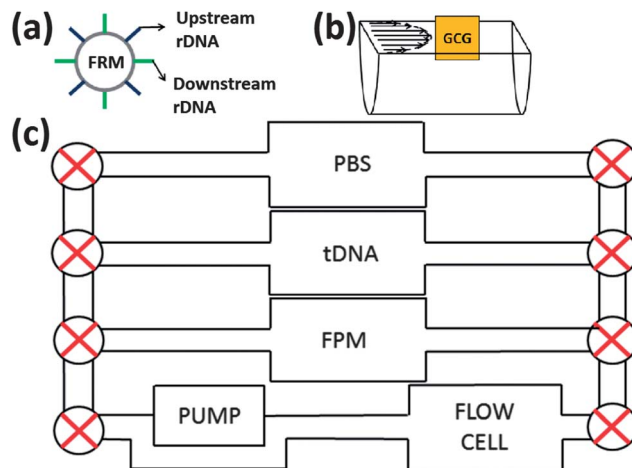


Fig. 4 (a) A schematic of a FPM coated with upstream and downstream rDNA, (b) a schematic of the flow cell where the GCG is placed at the center of laminar flow, and (c) a schematic of the flow system.

long, 3.5 mm wide, and 5.5 mm deep (volume = 356 μl and cross-section area = 19.25 mm²) driven with a peristaltic pump (model 77120-62, Cole-Parmer's Master Flex, Vernon Hills, IL). A schematic of the flow system is shown in Fig. 4c. An open container of deionized water was included in the incubator to control the humidity in the incubator to minimize evaporation from the open flow cell.

To examine the effects of both the temperature and the flow rate, we carried out hybridization experiments at various temperatures and various flow rates. The temperatures examined were room temperature (RT), 30 °C, and 35 °C, which were between the melting temperature of the WT, 23 °C, and that of the MT, 47 °C. The flow rates examined were 0, 2, 4, and 6 ml min⁻¹. At the given temperature and flow rate, we first circulated the MT or WT solution through the flow cell for 30 min for the MT or WT to bind to the pDNA on the GCG as illustrated by the schematic in Fig. 5a. Afterwards, we circulated the FRM suspension through the flow cell for 30 min to allow the FRMs to bind to the MT or WT captured on the GCG as schematically illustrated in Fig. 5b. PBS was then flowed through the flow cell to wash off loosely bound FRMs at a flow rate of 2 ml min⁻¹ for 30 min as schematically shown in Fig. 5c.

FRM counting

After washing, the GCG was air dried and examined using a fluorescent microscope (BX51, Olympus). The number of FRMs per unit area was determined with a custom made program written in MatLab as follows. The images taken in grayscale were turned into black and white using Otsu's method.³⁵ As the brightness of each FRM was different in each image (due to different exposure times and FRM fluorescence decay), the number of white pixels per FRM could be different in each image after black and white conversion. To determine the average number of white pixels per FRM, clusters of white pixels were labeled and cluster size distribution was determined. The

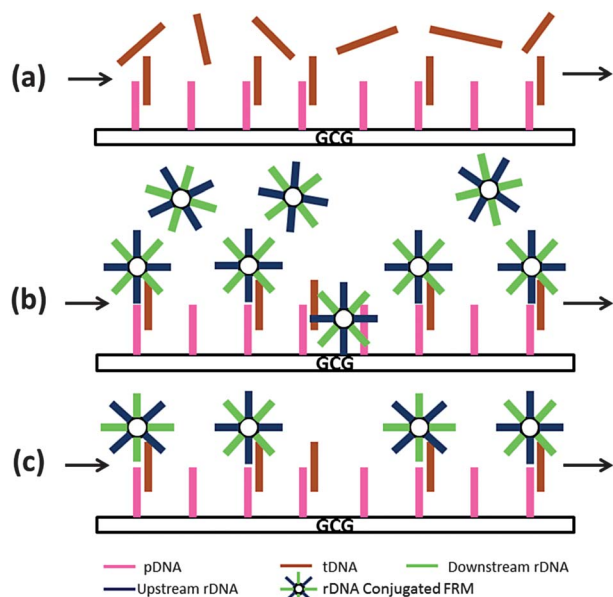


Fig. 5 A schematic of (a) tDNA sequence flowed over pDNA immobilized on a GCG, (b) upstream and downstream rDNA-conjugated FRMs flowed over the GCG surface and FRMs hybridized on the flanking regions of the tDNA sequences, and (c) unbound or loosely bound FRMs washed off from the GCG.

number of the FRMs per unit area in each image was determined from the pixel cluster size distribution as follows. First, clusters of white pixels less than 20 pixels were considered to be noise due to the gray-scale to black-white conversion and were not included in FRM counting. Second, in addition to well-separated FRMs, some FRMs were close together, they might appear as one large cluster. These large clusters of white pixels were separated from clusters of white pixels corresponding to single FRMs when determining the average number of white pixels per FRM. This was accomplished by applying an outlier removal algorithm (ASTM E178, $k = 1.5$, ASTM = American Society for Testing and Materials) with the large outlying clusters representing groups of FRMs that were too close to be seen as separate FRMs. After the large outlying groups of white pixels were neglected, the average FRM size in terms of the number of white pixels was determined by dividing the total number of white pixels in the remaining clusters by the total number of the remaining clusters. Once the average FRM size was determined, the total number of white pixels in all clusters including the large outliers was divided by this average number of white pixels per FRM to estimate the total number of FRMs per unit area.

It is worth noting that the rDNA immobilized on the FRM surface did not interfere with either the absorption or the emission of the FRMs as the absorption of DNAs occurred at wavelengths below 300 nm with a peak at 260 nm (ref. 36) whereas the absorption of FRMs occurred between 300 and 400 nm and the emission occurred above 400 nm. The present fluorescent images of the FRMs were also well validated by the bright-field images of the FRMs as the FRMs were visible in bright-field images (not shown) due to their large size.

Results

FRM conjugation and initial room-temperature testing without flow

In order to determine the optimal conditions for FRM conjugation to the rDNAs, different concentrations (3.3, 33, 330, and 3300 nM) were used to conjugate rDNAs as described above. To determine which concentration had the optimal conjugation conditions, we soaked GCGs with immobilized pDNAs in a $1 \mu\text{M}$ solution of the 200-nt MT followed by rinsing with PBS. We then soaked the GCGs in suspensions of rDNA-conjugated FRMs obtained with different rDNA concentrations over 30 min followed by rinsing with PBS. Fig. 6a shows the number of FRMs per mm^2 on the GCG surface versus the rDNA concentration for rDNA conjugation to the FRMs. As can be seen from Fig. 6a, the FRMs conjugated in 330 nM rDNA solution exhibited the most number of FRMs per mm^2 captured on the GCG surface under identical pDNA immobilization and tDNA hybridization conditions, indicating that the optimal rDNA concentration for the rDNA conjugation on the FRMs was 330 nM. The decrease in the number of FRMs hybridized at higher concentrations of rDNA is likely due to the increased steric hindrance associated with a higher rDNA density on the FRM surface, which reduced the hybridization efficiency of

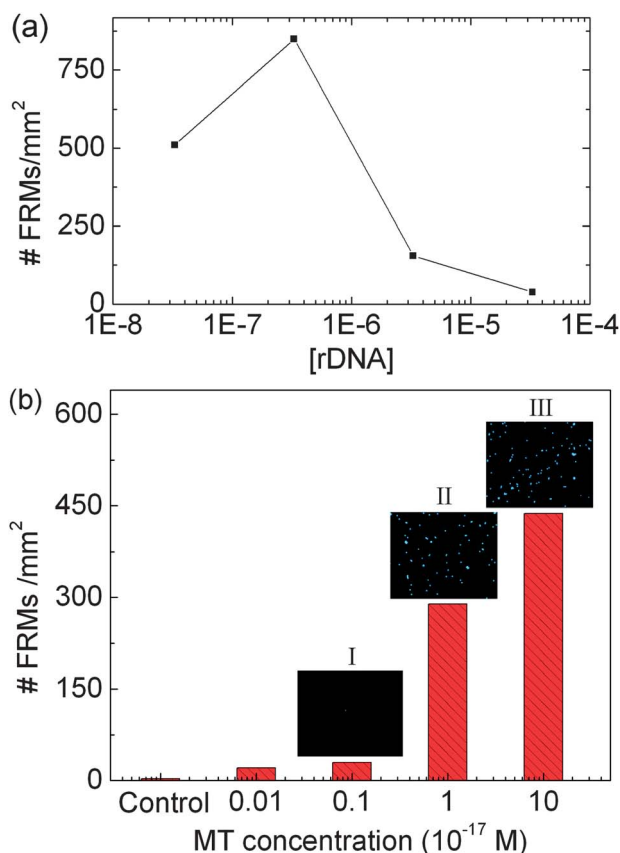


Fig. 6 Number of FRMs per mm^2 captured on the GCG (a) followed by 10^{-10} M MT detection versus rDNA concentration and, (b) followed by MT detection versus MT concentration with pDNA optimally immobilized in 330 nM pDNA. Both (a) and (b) were obtained at room temperature and without flow.

the FRMs with the captured DNA on the GCG surface.^{37–39} In what follows, all FRMs were conjugated with rDNAs at this concentration.

We then tested thus-obtained FRMs following MT hybridization to the GCG at various MT concentrations for 30 min followed by FRM binding at 2.1×10^5 particles per ml and for 30 min where binding of both MT and FRMs was carried out at room temperature without flow. The resulting number of FRMs per mm^2 versus MT concentration is plotted in Fig. 6b. As can be seen from Fig. 6b, at 10^{-16} M and 10^{-17} M of MT, the GCG showed about 450 and 300 FRMs per mm^2 , respectively while at 10^{-18} M and 10^{-19} M of MT tDNA, the number of FRMs per mm^2 was comparable to that of the negative control at 0 M of MT. Sample fluorescent images of FRMs obtained at 10^{-18} M, 10^{-17} M, and 10^{-16} M MT are shown in insets I, II, and III, respectively, indicating that the concentration sensitivity of this method without flow was about 10^{-17} M of MT.

Effect of flow rate and temperature

Combinations of 3 different temperatures (room temperature, 30 °C and 35 °C) and 4 different flow rates (no flow, 2, 4 and 6 ml min^{-1}) were studied. The MT or WT was first flowed for 30 min followed by the flow of FRMs over 30 min at the same temperature and flow rate, and finally washed with PBS at a flow rate of 2 ml min^{-1} at the same temperature as described above. The MT and the WT were kept at 10^{-10} M. The number of FRMs per mm^2 hybridized to the MT on the GCG surface, to the WT on the GCG surface and to the negative control versus flow rate at room temperature, 30 °C, and 35 °C are plotted in Fig. 7a–c. It is interesting to note from Fig. 7a that at RT, the flow increased the binding of both the MT and the WT in the 2–4 ml min^{-1} range but decreased the binding of both the MT and the WT as the flow rate increased. Such an increase of binding at a low flow rate and a decrease in binding upon further increase of flow rate were also observed in the *Bacillus anthracis* detection in ref. 21. The enhancement of binding by a flow has also been observed in antibody binding on antigen.⁴⁰ The enhanced binding at a lower flow rate was presumably because flow helped to bring more tDNAs to the GCG surface for binding. Without flow, the DNAs would have relied solely on diffusion to get to the GCG surface. While flow can help bring more tDNAs to the GCG surface, it could also generate an impingement force on the FRMs²¹ which could overcome the binding force between the tDNAs and pDNAs to unbind them from the GCG, thus reducing the overall number of FRMs bound on the GCG surface as the flow rate was further increased. At 30 °C and 35 °C, though, the binding of both the MT and the WT decreased monotonically with an increasing flow rate, presumably due to the weakening of the binding of the pDNA to both the MT and the WT. Although the binding of the pDNA to both the MT and WT decreased with an increasing flow rate at 30 °C and 35 °C, what was of interest is that the binding of the pDNA to the WT was suppressed to the levels similar to the negative controls at higher flow rates, suggesting that flow made the detection more selective at these two temperatures. In the following, we will refer to the number of FRMs per mm^2

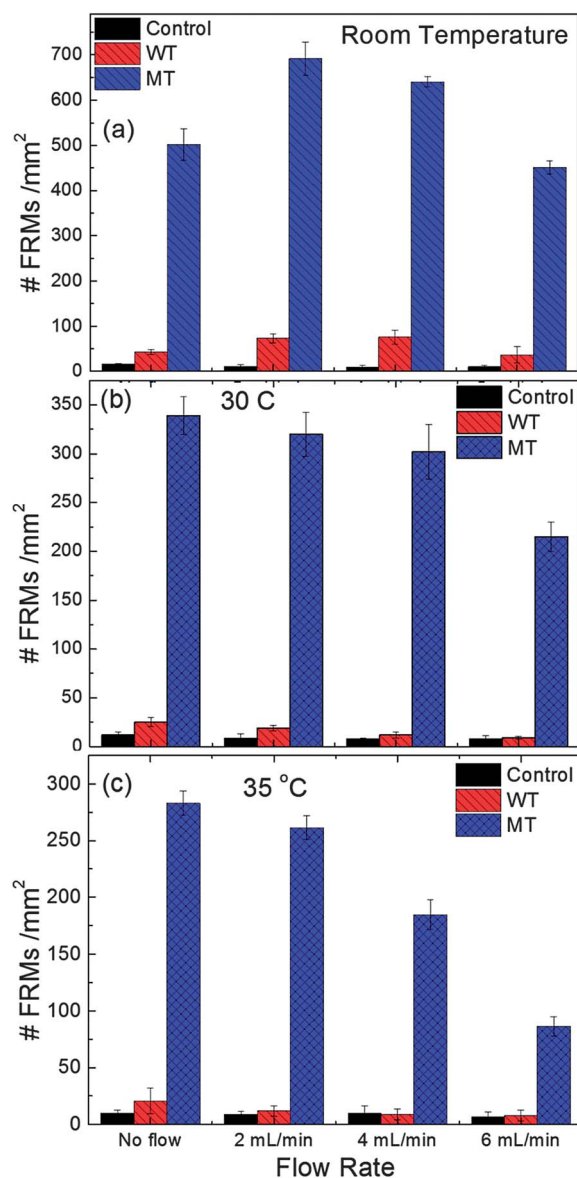


Fig. 7 Number of FRMs per mm^2 captured by a GCG followed by: detection in the control (no MT or WT, black); detection at 10^{-10} M WT (red); and detection at 10^{-10} M MT (blue). Detections were carried out in triplicate (a) at room temperature, (b) at 30 °C, and (c) at 35 °C.

captured on the GCG surface as the “signals”, S and S_{MT} , S_{WT} , and S_{C} , refer to the number of FRMs per mm^2 captured on the GCG surface following flowing a 10^{-10} M MT solution, a 10^{-10} M WT solution, and a control blank PBS, respectively. To examine whether the flow helped to increase the detection specificity, we plot the ratio, $S_{\text{WT}}/S_{\text{C}}$ versus flow rate in Fig. 8a with black for room temperature, red for 30 °C and blue for 35 °C. As can be seen, with flow, $S_{\text{WT}}/S_{\text{C}}$ was significantly reduced to close to unity not only at 35 °C but also at 30 °C. We further compared the S_{WT} and S_{C} using the Mann–Whitney U test.⁴¹ The resulting p value versus flow rate is plotted, again, with black for room temperature, red for 30 °C and blue for 35 °C. As can be seen, at low flow rates of 0 and 2 ml min^{-1} S_{WT} and S_{C} were statistically different ($p < 0.05$) at room temperature

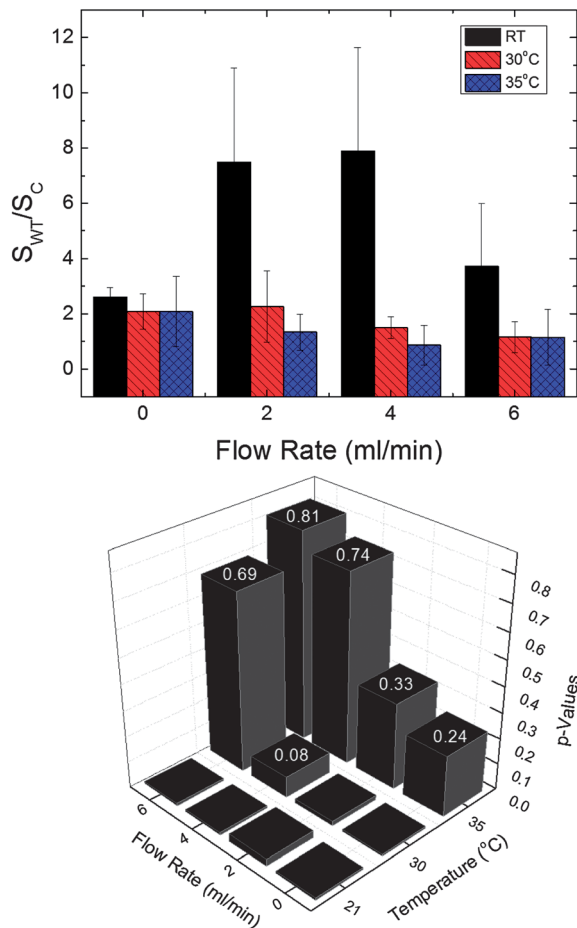


Fig. 8 (a) S_{WT}/S_C and (b) p value versus flow rate at room temperature (black), at 30 °C (red), and at 35 °C (blue) where S_{WT} and S_C are the numbers of FRMs per mm^2 captured by a GCG followed by detection at 10^{-10} WT and that captured by a GCG followed by detection in control (no WT or MT). Detections were carried out in triplicate.

and at 30 °C while at high flow rates of 4 and 6 ml min^{-1} S_{WT} and S_C were only statistically different at room temperature but not at 30 °C. These results indicated that the diminished significance of S_{WT} against S_C at a flow rate of 4–6 ml min^{-1} permitted specific MT detection at a lower temperature of 30 °C as opposed to 35 °C with a flow rate of 0–2 ml min^{-1} . One measure of MT detection specificity with respect to WT is S_{MT}/S_{WT} . In Fig. 9, we plot S_{MT}/S_{WT} versus flow rate for all three temperatures: room temperature (black), 30 °C (red) and 35 °C (blue). As can be seen, by increasing the temperature alone, S_{MT}/S_{WT} increased only slightly from about 11 to about 12 at 35 °C. With flow, S_{MT}/S_{WT} increased dramatically. More importantly, at 30 °C flow weakened the binding of WT more than that of MT to allow S_{MT}/S_{WT} to reach around 24 at 4 ml min^{-1} , which was higher than the S_{MT}/S_{WT} at any flow rate at 35 °C, indicating that flow could indeed enhance the detection specificity at a low temperature to allow more sensitive detection. The above results indicated that with the present flow setup the optimal detection conditions for the current HBV DM MT occurred at 30 °C and a flow rate of 4 ml min^{-1} .

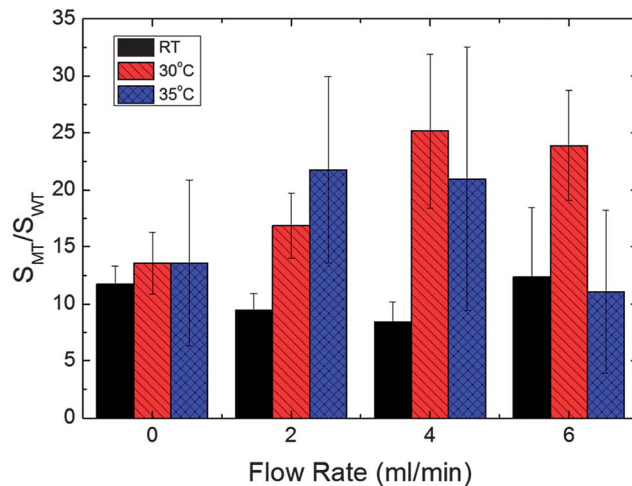


Fig. 9 S_{MT}/S_{WT} versus flow rate where S_{MT} is the number of FRMs per mm^2 captured by a GCG followed by detection at 10^{-10} MT and S_{WT} is the number of FRMs per mm^2 captured by a GCG followed by detection at 10^{-10} WT at room temperature (black), at 30 °C (red), and at 35 °C (blue). Detections were carried out in triplicate.

S_{MT}/S_{WT} at 10^3 , 10^6 , and 10^7 WT/MT concentration ratios

As can be seen from Fig. 6b, 10^{-17} M was the lowest MT concentration where the MT could be detected without flow by using the current detection scheme. To see how specific the MT detection was at this lowest detectable concentration, we used the optimal conditions, *i.e.*, 30 °C with a flow rate of 4 ml min^{-1} and carried out MT detection at 10^{-17} M for 30 min followed by 30 min of FRM hybridization. We then carried out WT detection at concentrations of 10^{-16} , 10^{-14} , 10^{-11} , and 10^{-10} M (*i.e.*, 10-fold, 10^3 -fold, 10^6 -fold, and 10^7 -fold that of the MT) followed by 30 min of FRM hybridization. In Fig. 10a, we plot the number of FRMs per mm^2 captured by the hybridized WT at different concentrations, with and without 4 ml min^{-1} flow rate (empty and pattern filled blue bars respectively) and the number of FRMs per mm^2 captured by the hybridized mixture of the same concentrations of WT and 10^{-17} M of MT with and without 4 ml min^{-1} flow rate (empty and pattern filled red bars respectively) versus WT concentration at 30 °C. Also plotted in Fig. 10a are the horizontal bars indicating the number of FRMs per mm^2 captured by hybridized 10^{-17} M of MT only, at 30 °C with and without 4 ml min^{-1} flow rate (violet and green respectively) and that non-specifically bound of control (brown). In Fig. 10b, we plotted the S_{MT}/S_{WT} and S_{MIX}/S_{WT} ratios with and without 4 ml min^{-1} flow rate deduced from Fig. 10a. As can be seen, without flow, S_{WT} remained different from S_C . With a flow of 4 ml min^{-1} , S_{WT} was not distinguishable from S_C . Moreover, mixture experiments showed that, at 30 °C, even the addition of 10^7 fold more amount of WT did not result in a significant increase in the number of hybridized FRMs, when 4 ml min^{-1} flow is applied. On the other hand, in the case of no flow, the number of FRMs hybridized increased significantly. Moreover specificity increased significantly under flow conditions with respect to no-flow conditions as can be seen from Fig. 10b, and mixing significantly high concentrations of WT into a solution of

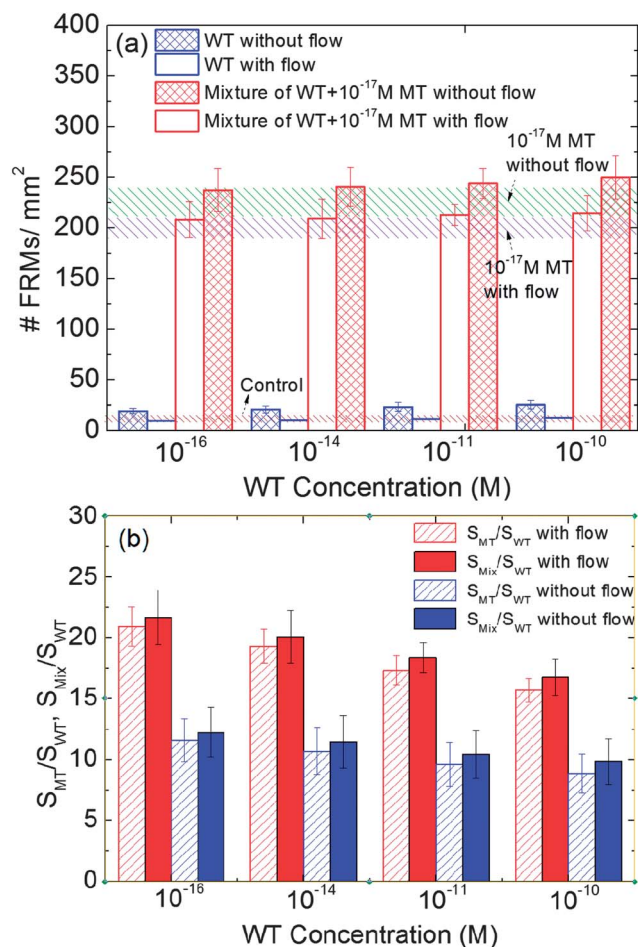


Fig. 10 (a) Number of FRMs per mm^2 versus WT concentration and, (b) ratio of the number of FRMs per mm^2 of MT/WT and mixture/WT versus WT where the mixture is 10^{-17} M MT mixed with different WT concentrations, and brown, blue and green horizontal bars represent the number of FRMs per mm^2 for control, 10^{-17} M MT with flow and 10^{-17} M MT without flow conditions. Both (a) and (b) are done at 30°C in 4 ml min^{-1} flow rate or under no flow conditions. Detections were carried out in triplicate.

10^{-17} M MT did not change this ratio. This indicates that the presence of WT of any concentration at 30°C and 4 ml min^{-1} had no discernible contribution to the detection signal even at a MT concentration as low as 10^{-17} M and that a flow of 4 ml min^{-1} made the detection as specific as 10^{-17} M MT/ 10^{-10} WT, or 1 MT to 10^7 WT.

Discussions

There were two main reasons for us to choose $6\ \mu\text{m}$ FRMs. Firstly, they are easily visible in an optical microscope. The fluorescent signals of the FRMs could be validated by the bright-field images of the FRMs. Secondly their relatively large size increased the impingement force induced on the FRMs bound on the surface by the flow. With a cross-sectional area of the detection chamber being $19.25\ \text{mm}^2$, the average flow velocity u was 1.7, 3.5 and $5.2\ \text{mm s}^{-1}$ for flow rates 2, 4, and $6\ \text{ml min}^{-1}$, respectively. The Reynolds number, $\text{Re} = \rho uv/\eta$, was just 6, 12, and 18 at flow rates 2, 4, and $6\ \text{ml min}^{-1}$, respectively where

$\rho = 1010\ \text{kg m}^{-3}$ was the density of the fluid, $\eta = 1.05\ \text{cP}$ the viscosity of the fluid and w the width of the flow cell, well in the range of laminar flow. Furthermore the entrance length, I_e , the length over which a fully developed velocity profile can be established once the flow entered the flow cell, can be calculated using:

$$I_e = 0.06d\text{Re}, \quad (1)$$

where d is the width of the flow cell. According to eqn (1) even at the highest flow rate which gave the largest Re, the entrance length was approximately 3.8 mm which was well below 7.7 mm, the distance from the inlet of the flow cell to GCG. Therefore, the flow in the detection chamber at the position of GCG was laminar and the flow velocity profile in the width direction was parabolic as schematically shown in Fig. 4b: u was zero at the cell wall and maximum at the center of the flow. Thus, unlike other systems where the capture surface is part of a wall of the flow channel,²¹ at which point the fluid velocity diminishes to zero, the present system situates the capture surface at the center of the flow where the flow velocity is at a maximum (as shown schematically in Fig. 4b). The concept of Goldman *et al.*,⁴² for a sphere parallel to a planar wall in a uniform flow, could be applied to the FRMs bound on the GCG in the middle of a laminar flow where the flow velocity was uniform as discussed above. According to Goldman *et al.*, in the middle of the flow cell where GCG is situated, one can obtain an analytical expression for the impingent force on a bound FRM as

$$F = (1.7)6\pi\eta a(1.5u), \quad (2)$$

where u is the average flow velocity and $1.5u$ is the flow velocity at the center of the flow, and $a = 3\ \mu\text{m}$ is the FRM radius. The deduced impingent force on the FRMs by the flow was about 262, 524, and 787 pN with $u = 1.7, 3.5$ and $5.2\ \text{mm s}^{-1}$ at 2, 4, and $6\ \text{ml min}^{-1}$, respectively. Although the exact binding forces between the pDNA and the WT and those between the pDNA and the MT were not known and it was unclear whether there were more than one captured MT or WT bound to a FRM, it suffices to say that the deduced force was consistent with 70–1500 pN found in the de-hybridization of a single double-stranded DNA.^{43,44}

It is also of interest to note that standard detection of methylations uses bisulfite to first convert unmethylated cytosines to uracils to create single-nucleotide mismatches not unlike single mutations.^{45,46} It is likely that the current methodology of using flow- and temperature-dependent FRM hybridization can be applied to detect methylations as well by designing probes for the methylated cytosine residues that are associated with a disease such as colon cancer.

Conclusions

We have investigated the effect of a laminar flow on enhancing the specificity of MT detection at a lower temperature by immersing the detection GCG surface at the center of the flow of

the target MT or WT at various flow rates and temperatures. pDNA complementary to the target MT DNA was immobilized on the GCG surface. 30 min of flow of the MT or WT DNA solution was followed by a flow of 6 μm FRMs of 10^5 FRMs per ml for 30 min at the same flow rate and temperature. With HBV DM as the model MT, we have shown that flow can increase the MT detection specificity by lowering the detection temperature to allow (1) a higher ratio of $S_{\text{MT}}/S_{\text{WT}}$ and (2) a lower S_{WT} not distinguishable from S_{C} . For the present system, a flow rate of 4–6 ml min^{-1} reduced the specific MT detection temperature from 35 °C without flow to 30 °C with a flow rate of 4–6 ml min^{-1} . Furthermore, optimal specific MT detection was shown to occur at a lower temperature with flow than the temperature without flow. For example, the detection specificity as measured by $S_{\text{MT}}/S_{\text{WT}}$ was 24 at 30 °C and 4 ml min^{-1} as opposed to 15 at 35 °C without flow. These results clearly indicate that flow can be utilized to help increase mutation detection specificity at a lower temperature.

Acknowledgements

This work was supported in part by the Coulter-Drexel Translational Research Partnership Grant and the Nanotechnology Institute (NTI), University Grant program of the Commonwealth of Pennsylvania's Ben Franklin Technology Development Authority through Ben Franklin Technology Partners of Southeast Pennsylvania. We would like to thank Dr Ying-Hsiu Su and Ms Selena Lin for many valuable discussions.

References

- 1 Y. H. Su, M. Wang, D. E. Brenner, A. Ng, H. Melkonyan, S. Umansky, S. Syngal and T. M. Block, *J. Mol. Diagn.*, 2004, **6**, 101–107.
- 2 R. Fodde and M. Losekoot, *Hum. Mutat.*, 1994, **3**, 83–94.
- 3 R. B. Scholz, K. Milde-Langosch, R. Jung, H. Schlechte, H. Kabisch, C. Wagener and T. Loning, *Hum. Mol. Genet.*, 1993, **2**, 2155–2158.
- 4 M. Orita, H. Iwahana, H. Kanazawa, K. Hayashi and T. Sekiya, *Proc. Natl. Acad. Sci. U. S. A.*, 1989, **86**, 2766–2770.
- 5 P. V. Danenberg, T. Horikoshi, M. Volkenandt, K. Danenberg, H. J. Lenz, L. C. Shea, A. P. Dicker, A. Simoneau, P. A. Jones and J. R. Bertino, *Nucleic Acids Res.*, 1992, **20**, 573–579.
- 6 G. Sarkar, H. S. Yoon and S. S. Sommer, *Nucleic Acids Res.*, 1992, **20**, 871–878.
- 7 D. Soto and S. Sukumar, *Genome Res.*, 1992, **2**, 96–98.
- 8 R. G. Cotton, N. R. Rodrigues and R. D. Campbell, *Proc. Natl. Acad. Sci. U. S. A.*, 1988, **85**, 4397–4401.
- 9 J. A. Saleeba and R. G. Cotton, *Nucleic Acids Res.*, 1991, **19**, 1712.
- 10 P. A. Roest, R. G. Roberts, S. Sugino, G. J. van Ommen and J. T. den Dunnen, *Hum. Mol. Genet.*, 1993, **2**, 1719–1721.
- 11 R. van der Lijst, P. M. Khan, H. Vasen, C. van Leeuwen, C. Tops, P. Roest, J. den Dunnen and R. Fodde, *Genomics*, 1994, **20**, 1–4.
- 12 R. J. Lipshutz, D. Morris, M. Chee, E. Hubbell, M. J. Kozal, N. Shah, N. Shen, R. Yang and S. P. Fodor, *BioTechniques*, 1995, **19**, 442–447.
- 13 E. M. Southern, *Trends Genet.*, 1996, **12**, 110–115.
- 14 G. H. Reed and C. T. Wittwer, *Clin. Chem.*, 2004, **50**, 1748–1754.
- 15 K. M. Ririe, R. P. Rasmussen and C. T. Wittwer, *Anal. Biochem.*, 1997, **245**, 154–160.
- 16 E. Lyon, *Expert Rev. Mol. Diagn.*, 2001, **1**, 92–101.
- 17 R. H. Lipsky, C. M. Mazzanti, J. G. Rudolph, K. Xu, G. Vyas, D. Bozak, M. Q. Radel and D. Goldman, *Clin. Chem.*, 2001, **47**, 635–644.
- 18 Y. You, B. G. Moreira, M. A. Behlke and R. Owczarzy, *Nucleic Acids Res.*, 2006, **34**, e60.
- 19 P. H. Rogers, E. Michel, C. A. Bauer, S. Vanderet, D. Hansen, B. K. Roberts, A. Calvez, J. B. Crews, K. O. Lau, A. Wood, D. J. Pine and P. V. Schwartz, *Langmuir*, 2005, **21**, 5562–5569.
- 20 Y. Zhang, V. T. Milam, D. J. Graves and D. A. Hammer, *Biophys. J.*, 2006, **90**, 4128–4136.
- 21 J. P. McGovern, W. Y. Shih, R. Rest, M. Purohit, Y. Pandya and W. H. Shih, *Analyst*, 2008, **133**, 649–654.
- 22 S. P. Mulvaney, C. L. Cole, M. D. Kniller, M. Malito, C. R. Tamanaha, J. C. Rife, M. W. Stanton and L. J. Whitman, *Biosens. Bioelectron.*, 2007, **23**, 191–200.
- 23 S. P. Mulvaney, C. N. Ibe, C. R. Tamanaha and L. J. Whitman, *Anal. Biochem.*, 2009, **392**, 139–144.
- 24 S. P. Mulvaney, K. M. Myers, P. E. Sheehan and L. J. Whitman, *Biosens. Bioelectron.*, 2009, **24**, 1109–1115.
- 25 C. C. Hsia, H. Yuwen and E. Tabor, *Lancet*, 1996, **348**, 625–626.
- 26 M. Baptista, A. Kramvis and M. C. Kew, *Hepatology*, 1999, **29**, 946–953.
- 27 P. Arbuthnot and M. Kew, *Int. J. Exp. Pathol.*, 2008, **82**, 77–100.
- 28 S. Y. Kuang, P. E. Jackson, J. B. Wang, P. X. Lu, A. Munoz, G. S. Qian, T. W. Kensler and J. D. Groopman, *Proc. Natl. Acad. Sci. U. S. A.*, 2004, **101**, 3575–3580.
- 29 S. Y. Kuang, S. Lekawanvijit, N. Maneekarn, S. Thongsawat, K. Brodovicz, K. Nelson and J. D. Groopman, *Cancer Epidemiol., Biomarkers Prev.*, 2005, **14**, 380–384.
- 30 X. D. Ren, S. Y. Lin, X. Wang, T. Zhou, T. M. Block and Y. H. Su, *J. Virol. Methods*, 2009, **158**, 24–29.
- 31 J. SantaLucia, Jr, *Proc. Natl. Acad. Sci. U. S. A.*, 1998, **95**, 1460–1465.
- 32 W. A. Kibbe, *Nucleic Acids Res.*, 2007, **35**, W43–W46.
- 33 M. C. Soylu, W.-H. Shih and W. Y. Shih, *Ind. Eng. Chem. Res.*, 2013, **52**, 2590–2597.
- 34 W. Wu, C. E. Kirimli, W. H. Shih and W. Y. Shih, *Biosens. Bioelectron.*, 2013, **43**, 391–399.
- 35 N. Otsu, *IEEE Trans. Syst. Man Cybern.*, 1979, **9**, 62–66.
- 36 J. M. Berg, J. L. Tymoczko, L. Stryer and L. Stryer, *Biochemistry*, W.H. Freeman, New York, 6th edn, 2007.
- 37 A. B. Steel, T. M. Herne and M. J. Tarlov, *Anal. Chem.*, 1998, **70**, 4670–4677.
- 38 A. W. Peterson, R. J. Heaton and R. M. Georgiadis, *Nucleic Acids Res.*, 2001, **29**, 5163–5168.

- 39 E. Huang, M. Satjapipat, S. Han and F. Zhou, *Langmuir*, 2001, **17**, 1215–1224.
- 40 J. Liu, N. J. Agrawal, A. Calderon, P. S. Ayyaswamy, D. M. Eckmann and R. Radhakrishnan, *Biophys. J.*, 2011, **101**, 319–326.
- 41 H. B. Mann and D. R. Whitney, *Ann. Math. Stat.*, 1947, **18**, 50.
- 42 A. J. Goldman, R. G. Cox and H. Brenner, *Chem. Eng. Sci.*, 1967, **22**, 653–660.
- 43 T. Strunz, K. Oroszlan, R. Schafer and H. J. Guntherodt, *Proc. Natl. Acad. Sci. U. S. A.*, 1999, **96**, 11277–11282.
- 44 G. U. Lee, L. A. Chrisey and R. J. Colton, *Science*, 1994, **266**, 771–773.
- 45 M. Frommer, L. E. McDonald, D. S. Millar, C. M. Collis, F. Watt, G. W. Grigg, P. L. Molloy and C. L. Paul, *Proc. Natl. Acad. Sci. U. S. A.*, 1992, **89**, 1827–1831.
- 46 O. El-Maarri, *Adv. Exp. Med. Biol.*, 2003, **544**, 197–204.